

EVALUATING AN ALTERNATIVE METHOD OF CALCULATING UPDRAFT HELICITY

Jeffrey M. Milne^{1,2,3*}, Israel L. Jirak³, and Harold E. Brooks⁴

¹*Cooperative Institute for Severe and High-Impact Weather Research and Operations*

²*University of Oklahoma, School of Meteorology*

³*NOAA/NWS/NCEP Storm Prediction Center*

⁴*NOAA/OAR National Severe Storms Laboratory*

1. INTRODUCTION

Updraft helicity (UH) was introduced as a forecasting parameter by Kain et al. (2008). It is mathematically defined as the vertical integral of the product of vertical velocity and vertical vorticity over a specified vertical layer. In a mathematical sense,

$$UH = \int_{z_1}^{z_2} w\zeta dz, \quad (1)$$

where z_1 and z_2 are the lower and upper bounds of the vertical layer, w is vertical velocity, and ζ is vertical vorticity.

A commonly chosen vertical layer in severe weather forecasting is 2-5km, because "the primary interest is on storm rotation in the lower to middle troposphere" (Kain et al. 2008). Updraft helicity reduces the 3-d wind field to a single number to identify rotating updrafts. While this approach is useful to forecasters, Milne et al. (2018) showed that $w\zeta$ existed outside of the commonly used 2-5km layer.

Fixed-layer 2-5km UH has shown utility in forecasting all severe hazards (tornadoes, strong wind, and large hail; Sobash et al. 2011). Filtering fixed-layer 2-5km UH using environmental parameters has also been shown to be useful in forecasting tornadoes (Gallo et al. 2016).

Outside of the 2-5km layer, a fixed 0-3km UH has also been used as a proxy for low level rotation to forecast tornadoes (Sobash et al. 2016).

Milne et al. (2018) showed that, in addition to $w\zeta$ existing outside of the 2-5km layer, both positive and negative $w\zeta$ existed within the same updraft. There was also considerable variation in the vertical structure of $w\zeta$ among different storms.

Milne et al. (2020) proposed a variable-layer UH calculation, which integrates from the surface to the lowest level of downward vertical velocity. This variable-layer calculation was shown in idealized supercell and squall line simulations to have higher magnitudes than fixed-layer UH.

*Corresponding author address: 120 David L. Boren Blvd, Ste 2100, Norman, OK 73072;
E-mail: jeffrey.milne@noaa.gov.

Model Version	v3.4.1
Grid spacing	3km
Vertical levels	35
Time step	24s
Boundary layer	MYJ
Microphysics	WSM6
Longwave	RRTM
Shortwave	Dudhia
LSM	Noah
Initial conditions	40km NAM

TABLE 1. WRF model configuration

This study implements the variable-layer UH calculation proposed in Milne et al. (2020) and applies it to real world simulations. The variable and fixed-layer calculations will be compared objectively.

2. DATA AND METHODS

2.1. Model details

To compare the performance of fixed- and variable-layer UH, WRF was run (configuration summarized in Table 1, as in the NSSL-WRF) for 3 April 2014, 11 May 2014, 8 April 2015, 16 May 2015, and 15 February 2016. Tornadoes occurred on all five days. The model was initialized at 00 UTC and ran for 36 hours. Hourly maximum fixed- (2-5km) and variable-layer UH were output and aggregated to create 24-hour maximum fields from 12 UTC to 12 UTC (forecast hours 12-36).

2.2. Variable-layer UH calculation

The variable-layer UH calculation, proposed in Milne et al. (2020), is

$$UH_{variable} = \int_0^{z_{w<0}} w\zeta dz, \zeta > 0 \quad (2)$$

where w and ζ are as in Equation 1, and $z_{w<0}$ is the lowest level of downward w . This calculation only considers $\zeta > 0$ to account for situations in which both positive and negative ζ exist in the same column, as shown in Milne et al. (2018). There is no

magnitude threshold on the downward w limit; any layer in which $w < 0$ will stop the calculation. The goal of the variable-layer calculation is the capture the full depth of rotating updrafts. Both because variable UH only counts positive $w\zeta$ and because it captures the entire depth of the updraft, it should almost always have a higher magnitude than fixed-layer UH. The only case in which fixed-layer UH has a higher magnitude is when there is a low level ($< 2\text{km}$) downward w , which stops the variable calculation and is ignored by the fixed calculation.

2.3. Objective Verification

Tornado reports were collected from *Storm Data* for each day. The UH forecasts were objectively verified using a neighborhood approach. Hits were counted for any tornado report within 39km of a grid square with a UH magnitude above a specified threshold. Misses were counted for any tornado report that was not counted as a hit. False alarms were counted for any grid square with a UH magnitude above a specified threshold that was not with 39km of a tornado report. Correct nulls were counted for any grid square not counted in any other category, subject to a mask that only included grid squares that had a forecast rainfall greater than 0.01".

A performance diagram (Roebber 2009) was used to display the verification results. In addition, area under the precision-recall curve (AUC-PR, a precision-recall curve is identical to a performance diagram with the axes flipped) was calculated, since AUC-PR is a better metric for rare events than area under a receiver operating characteristic curve (Sofaer et al. 2019). Though it has limitations, a receiver operating characteristic curve (ROC curve) was also created, and the area under the ROC curve computed (AUC-ROC; Mason 1982; Harvey et al. 1992)

3. RESULTS

3.1. Bulk Verification

The bulk performance diagram for all five days can be seen in Figure 1. In bulk, the variable-layer UH outperformed the fixed-layer UH. However, upon examination of the verification for each day, it can be seen that fixed-layer UH outperforms variable-layer UH for all but one day. The improvements from the one day on which variable-layer UH performed better were enough to give variable-layer

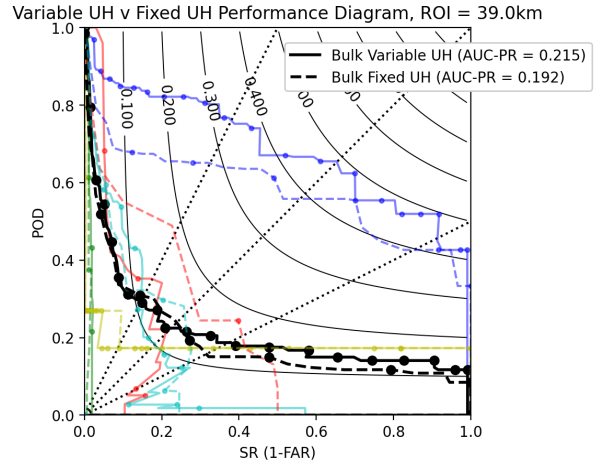


FIG. 1. Performance diagram showing bulk verification across a range of UH thresholds for all five days (dark black lines) and individual verification for each day (light colored lines, solid indicated variable-layer UH and dashed indicates fixed-layer UH). Thresholds start at zero and increase in increments of $10\text{m}^2\text{s}^{-2}$ for both variable and fixed-layer UH. Dots are plotted every $50\text{m}^2\text{s}^{-2}$. The green lines represent 3 April 2014; the blue lines represent 11 May 2014; the yellow lines represent 8 April 2015; the teal lines represent 16 May 2015; and the red lines represent 15 February 2016.

UH a higher AUC-PR in bulk than fixed-layer UH.

In bulk, variable-layer UH appears to outperform fixed-layer UH at the higher thresholds, which may indicate that variable-layer UH is identifying and highlighting the strongest storms with the greatest potential for producing tornadoes.

A ROC curve is shown in Figure 2. Note that the x-axis is zoomed in to only show POFD from 0-0.1 since there are only a few data points for high POFD (and thus low UH thresholds). While variable-layer UH has a higher AUC-ROC than fixed-layer UH, much of that difference is driven at the lowest thresholds. Closer examination of the curves reveals that variable-layer UH generally has higher POD for a given POFD than fixed-layer UH. This pattern also holds when examining individual days.

3.2. Individual Case: 16 May 2015

For this case, both methods miss the tornado reports in southern Minnesota (variable UH in Figure 3 and fixed UH in Figure 4). Both methods subjectively perform better in the southern half of the do-

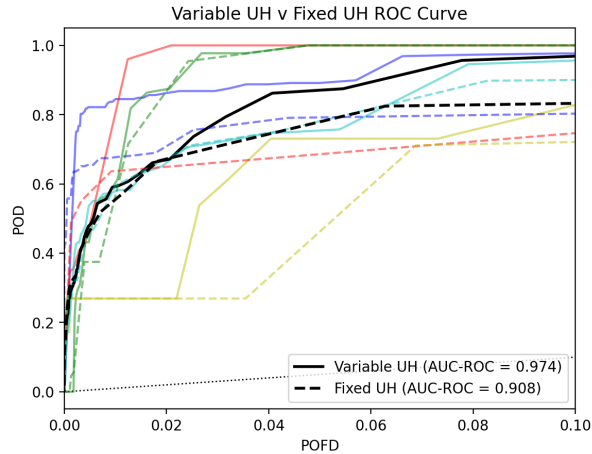


FIG. 2. As in Figure 1, but for a ROC curve. Note the x-axis only goes from 0-0.1.

main, with swaths of UH near the tornado reports in northeastern Oklahoma and southwestern Missouri. Variable-layer UH has higher values in general across the domain (Figure 5), with the greatest increases occurring in northeastern Oklahoma, southeastern Kansas, southwestern Missouri, and northwestern Arkansas.

A log-log scatter plot comparing the values of fixed and variable UH at each grid point is shown in Figure 6. For the most part, variable UH has higher magnitudes than fixed UH; the grid points in which fixed UH has a higher magnitude will need further examination. While the magnitudes of variable UH are in general higher than fixed UH, the differences appear to be the greatest for the highest magnitudes of fixed UH. This suggests that the most intense simulated storms are being highlighted even more in variable UH. This difference may be useful when forecasting by identifying the strongest simulated storms.

Because of the subjectively different performance in the different parts of the domain, it was decided to verify the northern and southern halves of the domain separately. To do this, the domain was split at 40°N and separate verification metrics were calculated north and south of 40°N. A performance diagram with those metrics is shown in Figure 7. In the full domain and both smaller domains, the fixed-layer UH outperforms the variable-layer UH in terms of AUC-PR. As expected from the subjective performance, the scores for the southern domain were much higher than both the full and northern domains.

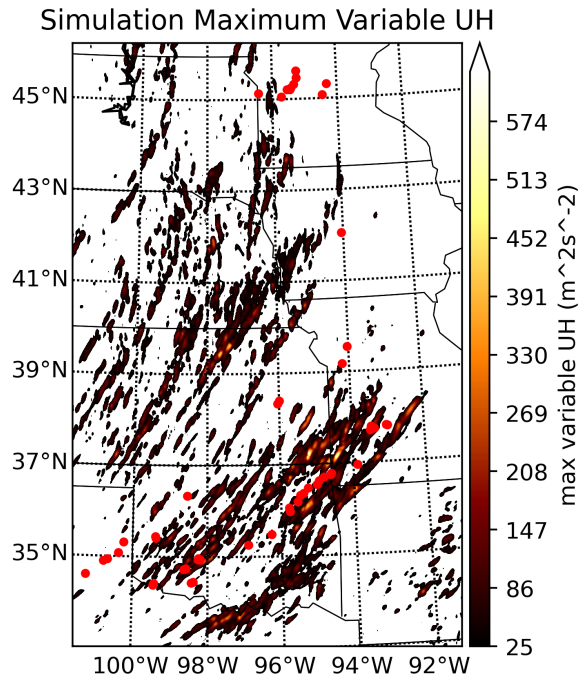


FIG. 3. Simulation maximum variable-layer UH for 16 May 2015. Red dots indicate tornado reports.

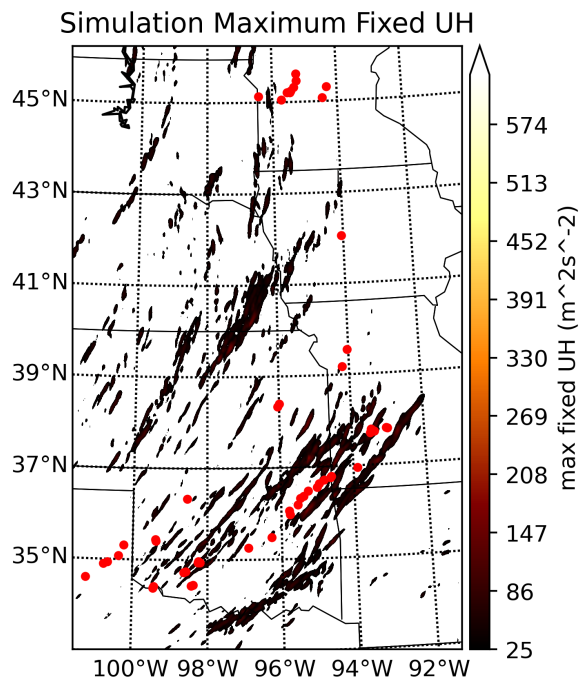


FIG. 4. As in Figure 3 but for fixed-layer UH.

Difference Between Variable UH and Fixed UH

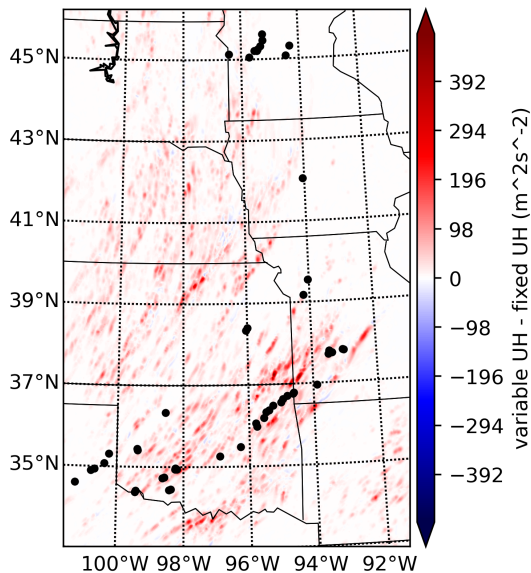


FIG. 5. Difference between variable and fixed-layer UH for 16 May 2015. Red indicates regions in which variable-layer UH had a higher magnitude than fixed-layer UH. Black dots indicate tornado reports.

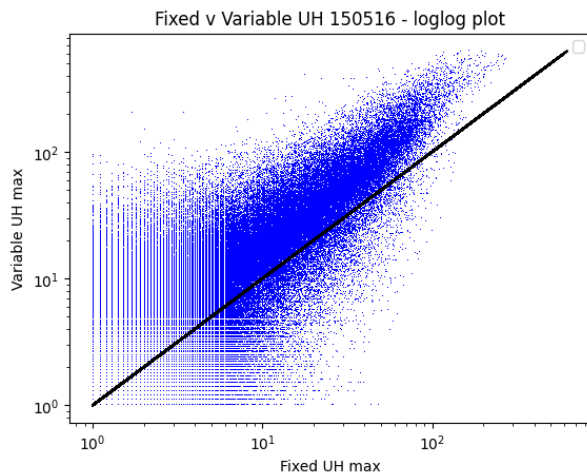


FIG. 6. A log-log scatter plot comparing the values of fixed and variable UH at a given grid point.

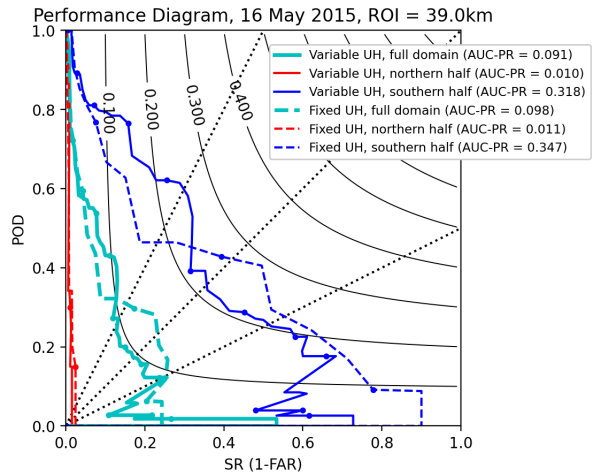


FIG. 7. Performance diagram for 16 May 2015, showing results for fixed- and variable-layer UH in dashed and solid, respectively, for the full domain, the domain north of 40°N, and the domain south of 40°N in teal, red, and blue, respectively.

This suggests that the performance of the two UH calculations is limited by the performance of the model. The model struggled to produce storms at all in the northern half of the domain, so both UH calculations scored poorly there. In the southern half of the domain, however, the model produced more storms, some of which were near tornado reports.

4. CONCLUSIONS AND FUTURE WORK

In bulk, variable-layer UH outperforms fixed-layer UH when using both AUC-PR and AUC-ROC. Closer investigation reveals that there was only one case in which variable-layer UH outperformed fixed-layer UH in terms of AUC-PR. This suggests that there may be certain cases in which variable UH outperforms fixed UH.

As expected, variable-layer UH has higher magnitudes than fixed-layer UH, and it subjectively can highlight regions that are potentially more favorable for rotating updrafts. Variable UH can also highlight the most intense simulated storms of the forecast. Verifying against EF2+ reports may highlight a potential benefit of the variable-layer UH calculation.

The major limitation of both calculations is the underlying model performance. If the model does not produce any storms, there will be no UH swaths no matter how UH is calculated. Within an individual case, it was shown that performance of both UH

calculations can vary across the domain depending on whether the model produced storms. However, even when sub-setting the domain, the relative performance of the two calculations did not change.

Ongoing work includes identifying cases in which variable-layer UH outperforms fixed-layer UH. Based on the calculation methods, this should be cases with shallow updrafts with a downward w somewhere in the 2-5km layer, which would zero out the fixed-layer calculation, and in cases with very deep updrafts extending well beyond the 2-5km layer. Situations in which fixed UH has a higher magnitude than variable UH will also be explored.

Environmental filtering is also being explored as a method to improve the variable-layer UH performance, since it has already been shown to improve fixed-layer UH performance (Gallo et al. 2016). Environmental filtering is also more appropriate to use when verifying based on tornado reports, to avoid penalizing the model for identifying high-based or elevated rotating storms that have little to no chance of producing a tornado. The definition of the variable-layer is also being explored, to potentially include environmental information in the definition of the variable-layer.

This research used a neighborhood approach for verification; object-based verification is also being explored to better identify and match swaths of tornado reports with UH swaths.

Acknowledgments. Some of the computing for this project was performed at the OU Supercomputing Center for Education & Research (OSCER) at the University of Oklahoma (OU). This extended abstract was prepared by Jeffrey Milne with funding provided by NOAA/Office of Oceanic and Atmospheric Research under NOAA-University of Oklahoma Cooperative Agreement #NA21OAR4320204, U.S. Department of Commerce. The statements, findings, conclusions, and recommendations are those of the author(s) and do not necessarily reflect the views of NOAA or the U.S. Department of Commerce.

REFERENCES

Gallo, B. T., A. J. Clark, and S. R. Dembek, 2016: Forecasting Tornadoes Using Convection-Permitting Ensembles. *Weather and Forecasting*, **31** (1), 273–295, doi:10.1175/WAF-D-

15-0134.1, URL <http://journals.ametsoc.org/doi/10.1175/WAF-D-15-0134.1>.

Harvey, L. O., K. R. Hammond, C. M. Lusk, and E. F. Mross, 1992: The application of signal detection theory to weather forecasting behavior. *Monthly Weather Review*, **120** (5), doi:10.1175/1520-0493(1992)120<0863:TAOSDT>2.0.CO;2.

Kain, J. S., and Coauthors, 2008: Some Practical Considerations Regarding Horizontal Resolution in the First Generation of Operational Convection-Allowing NWP. *Weather and Forecasting*, **23** (5), 931–952, URL <http://journals.ametsoc.org/doi/abs/10.1175/WAF2007106.1>.

Mason, I., 1982: A model for assessment of weather forecasts. *Australian Meteorological Magazine*, **30** (4).

Milne, J. M., I. L. Jirak, and H. E. Brooks, 2018: Investigating the Vertical Structure of Updraft Helicity in Convection-Allowing Models. *29th Conference on Severe and Local Storms*, Stowe, VT, URL <https://ams.confex.com/ams/29SLS/webprogram/Paper348472.html>.

Milne, J. M., I. L. Jirak, and H. E. Brooks, 2020: Investigating the Vertical Structure of Updraft Helicity in Convection-Allowing Models. *30th Conference on Weather Analytics and Forecasting/26th Conference on Numerical Weather Prediction*, Boston, MA, URL <https://ams.confex.com/ams/2020Annual/webprogram/Paper366087.html>.

Roebber, P. J., 2009: Visualizing Multiple Measures of Forecast Quality. *Weather and Forecasting*, **24** (2), 601–608, doi:10.1175/2008WAF2222159.1, URL <http://journals.ametsoc.org/doi/abs/10.1175/2008WAF2222159.1>.

Sobash, R. A., J. S. Kain, D. R. Bright, A. R. Dean, M. C. Coniglio, and S. J. Weiss, 2011: Probabilistic Forecast Guidance for Severe Thunderstorms Based on the Identification of Extreme Phenomena in Convection-Allowing Model Forecasts. *Weather and Forecasting*, **26** (5), 714–728, doi:10.1175/WAF-D-10-05046.1, URL <https://journals.ametsoc.org/doi/pdf/10.1175/WAF-D-10-05046.1> <http://journals.ametsoc.org/doi/abs/10.1175/WAF-D-10-05046.1>.

Sobash, R. A., G. S. Romine, C. S. Schwartz, D. J. Gagne, and M. L. Weisman, 2016: Explicit Forecasts of Low-Level Rotation from Convection-Allowing Models for Next-Day Tor-

nado Prediction. *Weather and Forecasting*, **31 (5)**, 1591–1614, doi:10.1175/WAF-D-16-0073.1, URL <http://journals.ametsoc.org/doi/10.1175/WAF-D-16-0073.1>.

Sofaer, H. R., J. A. Hoeting, C. S. Jarnevich, and C. R. Helen Sofaer, 2019: The area under the precision-recall curve as a performance metric for rare binary events. *Methods Ecol Evol*, **10**, doi:10.1111/2041-210X.13140.